iScience

CellPress
OPEN ACCESS

Article

Hydrogen co-production via nickel-gold electrocatalysis of water and formaldehyde

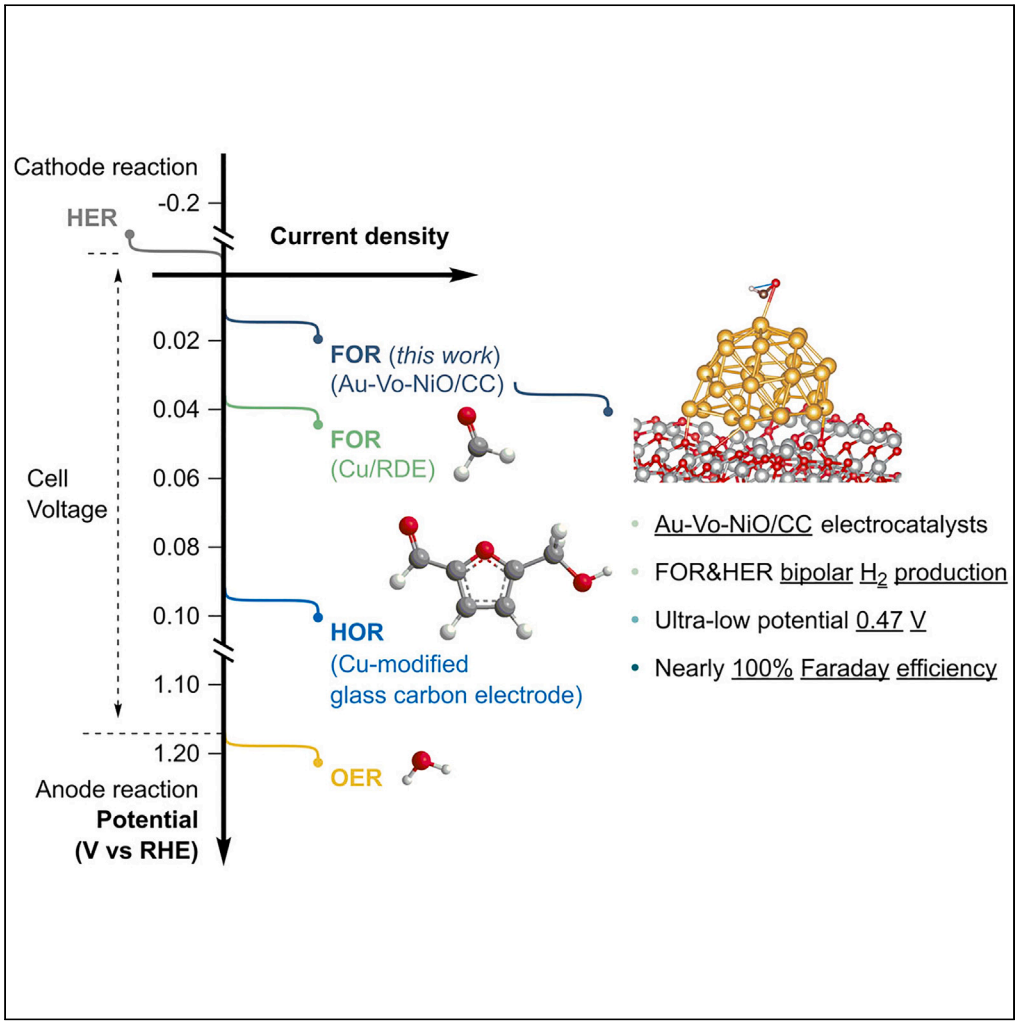

Zhixin Li, Yan Zhang, Qianqian Yang, ..., Fengzhan Si, Jing Zhao, Jiean Chen

jingzhao@nju.edu.cn (J.Z.)
chenja@szbl.ac.cn (J.C.)

Highlights

Design and synthesis of the new Au-Vo-NiO/CC electrocatalyst

Oxygen vacancies on the Ni nanostructure boost the catalytic performance of Au

Bipolar H_2 production is triggered at 0.47 V (vs. RHE) with a 100% Faraday efficiency

An 8-h long-term experiment confirms the electrode stability

Li et al., iScience 26, 107994
October 20, 2023
https://doi.org/10.1016/j.isci.2023.107994

iScience

CellPress
OPEN ACCESS

Article

Hydrogen co-production via nickel-gold electrocatalysis of water and formaldehyde

Zhixin Li,[1,5] Yan Zhang,[2,5] Qianqian Yang,[2] Jindong Wu,[2] Zhi Ren,[3] Fengzhan Si,[4] Jing Zhao,[1,*] and Jiean Chen[2,6,*]

SUMMARY

Hydrogen is one of the most promising future energy sources due to its highly efficient energy storage and carbon-free features. However, the energy input required for a hydrogen production protocol is an essential factor affecting its widespread adoption. Water electrolysis for hydrogen production currently serves a vital role in the industrial field, but the high overpotential of the oxygen evolution reaction (OER) dramatically impedes its practical application. The formaldehyde oxidation reaction (FOR) has emerged as a more thermodynamically favorable alternative, and the innovation of compatible electrodes may steer the direction of technological evolution. We have designed Au-Vo-NiO/CC as a catalyst that triggers the electrocatalytic oxidation of formaldehyde, efficiently producing H_2 at the ultra-low potential of 0.47 V (vs. RHE) and maintaining long-term stability. Integrated with the cathodic hydrogen evolution reaction (HER), this bipolar H_2 production protocol achieves a nearly 100% Faraday efficiency (FE).

INTRODUCTION

Molecular hydrogen is the smallest energy storage unit available to humanity. The evolution of an entire system integrating both the production and application of H_2 has emerged as one of the most promising strategies with which to respond to an energy crisis in the future.[1–6] Hydrogen fuel cells have depicted a practical application paradigm of this carbon-free energy, but their production aspect still needs continuous efforts from scientists.[7,8] Water electrolysis, theoretically an ideal alternative to fossil fuels for supplying H_2, involves the splitting of water into H_2 hydrogen evolution reaction (HER) and O_2 oxygen evolution reaction (OER).[9] However, the anodic OER, a four-electron transfer process, has sluggish reaction kinetics,[10] meaning that a relatively high voltage input (> 1.23 V vs. RHE) and energy consumption are needed to initiate water electrocatalysis.[11] A burgeoning research area focuses on combining an organic oxidation reaction with HER to complete an electron-flow circuit,[12] requiring relatively low overpotential to realize cathodic H_2 production. The organic compounds for anodic oxidation have a more favorable thermodynamic bias than water.[13] They can be converted into valuable organic backbones rather than oxygen,[14] avoiding the coexistence of hydrogen and oxygen while balancing the initial resource investment.[15,16] The concept has been validated in the iteratively upgraded platform for the electrolysis of biomass-derived chemicals such as glucose,[17] furfural,[1] and similar small molecules.[18–22] However, a high-voltage input is often necessary (> 1 V vs. RHE),[14,23,24] and the organic compounds commonly face solubility issues in a water medium, limiting scaled-up H_2 production. At this stage, formaldehyde (HCHO), an organic molecule with a high hydrogen content, is steadily emerging as a research focus.[1,25–27]

Formaldehyde is an efficient H-storage medium in an aqueous base system, with a thermodynamic preference for producing H_2. One of the manipulations in this regard depends on the C-H cleavage mediated by nanometal catalysts, such as Cu,[26,27] Ag,[25] Au,[28,29] and Pd.[28,30] The electrochemical oxidation of formaldehyde, triggered by metallic electrodes, has also been investigated, and currently, most studies focus on copper as an intrinsic activation site. According to theoretical calculations, the orbital overlap of the critical reaction intermediate $H_2C(OH)O^*$ with an active metal core dominates the energy gaps for several of the following reaction steps on the electrode surface: adsorption of the active intermediate, C-H cleavage, and Tafel recombination of the hydrogen atom.[27] Silver, having a 4*d* orbital, could interact with the O-atom (2*p* orbital) better than copper (3*d* orbital), thus providing a relatively low activation energy barrier.[25] Group IB metals have demonstrated catalytic activity toward the formaldehyde oxidation reaction (FOR). However, little research has focused on gold-mediated bipolar H_2 production.[31,32] We believe that, given the increased atomic radius and decent O-affinity of the Au catalyst, a complementary

[1]State Key Laboratory of Coordination Chemistry, Chemistry and Biomedicine Innovation Center (ChemBIC), School of Chemistry and Chemical Engineering, Nanjing University, Nanjing 210023, China
[2]Pingshan Translational Medicine Center, Shenzhen Bay Laboratory, Shenzhen 518055, China
[3]College of Pharmacy, Shenzhen Technology University, Shenzhen 518055, China
[4]Shenzhen Key Laboratory of Energy Electrocatalytic Materials, Shenzhen Key Laboratory of Polymer Science and Technology Guangdong Research Center for Interfacial Engineering of Functional Materials, College of Materials Science and Engineering, Shenzhen University, Shenzhen 518060, China
[5]These authors contributed equally
[6]Lead contact
*Correspondence: jingzhao@nju.edu.cn (J.Z.), chenja@szbl.ac.cn (J.C.)
https://doi.org/10.1016/j.isci.2023.107994

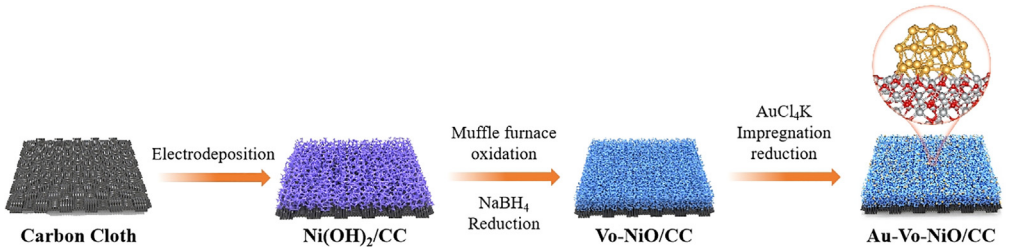

Scheme 1. The schematic diagram of the synthesis pathway for Au-Vo-NiO/CC

strategy could be envisaged for this field, representing a new trial involving formaldehyde-water co-electrolysis to realize simultaneous H_2 production at the cathode and anode. A new Au-containing electrode is also expected to deliver consistent performance over a more extended catalytic period than Cu at high current densities. Here, we designed a catalyst based on nickel (Ni), a metal with high electron transport capability, and introduced oxygen vacancies to enhance its electron transport rate. Previous studies have shown that oxygen vacancies can modify the electronic structure of the catalyst, creating new energy levels that facilitate efficient electron transport. Moreover, oxygen vacancies can increase the adsorption and activation of reaction substrates, thus expanding the number of active sites and promoting the catalytic reaction. Oxygen vacancies can also alter the surface morphology of the catalyst, affecting the binding mode of the substrates and changing the catalytic activity.[33] For catalysts loaded with precious metals, oxygen vacancies can reduce the metal loading while maintaining the catalytic performance.

In this work, we successfully synthesized the new Au-Vo-NiO/CC catalyst containing oxygen vacancies,[34] by docking a small amount of Au to serve as the FOR active catalytic site. A sophisticated balance between FOR and HER was achieved for bipolar H_2 production under alkaline conditions. The electrocatalytic cycle runs smoothly at a potential as low as 0.47 V (vs. RHE) when the current density reaches 100 mA cm^{-2}, producing hydrogen with a 100% Faraday efficiency.

RESULTS AND DISCUSSION

Materials characterization

The core material for this study is the electrocatalyst Au-Vo-NiO/CC (Scheme 1). This catalyst was prepared by combining electrodeposition and impregnation reduction using carbon cloth as the primary support material and nickel nitrate and potassium chloroaurate as raw materials. Au/CC and NiO/CC catalysts were applied as the direct reference objects for comparative studies.

Scanning electron microscopy (SEM) was used to characterize the microscopic nanostructures of the electrocatalyst Au-Vo-NiO/CC and the precursors $Ni(OH)_2$/CC, NiO/CC and Vo-NiO/CC. The results revealed the structural changes during the synthetic process (Figures 1A–1C). $Ni(OH)_2$ was grown *in situ* on the carbon cloth by electrodeposition, forming irregular nano-sheets with the metal Ni atoms precisely coupled to the carbon fibers. The resulting structure is well-situated for the efficient shuttle of electrons. $Ni(OH)_2$ was oxidized into NiO nanoflakes by calcination at 350°C under an air atmosphere. After treatment with sodium borohydride, the SEM images of Vo-NiO/CC showed a significant increase in their surface pits. The initially smooth surface became rough, and slight local spalling occurred. This indicates that the surface structure of the catalytic material has changed after treatment with sodium borohydride, facilitating the growth of reduced Au nanoparticles by subsequent impregnation. This could also induce the generation of oxygen vacancies in the material, exposing more active sites and improving the catalytic activity. SEM images of Au-Vo-NiO/CC showed that Au was growing *in situ* on the surface of NiO nanosheets in nanoparticles, with diameters of about 100 nm. This structure could efficiently facilitate the FOR at a low Au-loading level, taking advantage of the electron transport properties of Ni. The microstructure was examined by transmission electron microscopy (TEM), suggesting fantastic lattice stripes with an interplanar spacing of 2.088 nm and 2.355 nm corresponding to NiO (111) and Au (202) crystal planes of a cube (Figures 1D and 1F). According to the EDS energy spectra, Ni and O were uniformly spread on the surface of the carbon cloth, and the nanosheets were composed of elemental Au (Figures 1H–1K). The elemental percentages of O: Ni: Au distributed on the catalyst surface are 59:37:4, demonstrating that Au is attached to the NiO surface at a low loading rate (Figures S1 and S2).

X-ray photoelectron spectroscopy (XPS) was used to analyze the chemical composition of the Au-Vo-NiO/CC catalyst, and the results showed that nickel, gold, and oxygen elements are all distributed on the catalyst surface (Figures 2A and S3). The two peaks at 83.2 and 86.9 eV for the element Au are from Au^0 (Figure 2B).[35,36] The fitting of the Ni 2*p* XPS high-resolution spectra shows that Ni mainly exists in Ni2+ in the catalyst, but there is still a tiny amount of Ni^0 (Figure 2C). This result is consistent with the X-ray diffraction (XRD) characterization data, which shows that the diffraction peaks at 37.25, 43.29, 63.93, and 75.42 can be attributed to NiO(PDF#897101).[21] The diffraction peaks at 38.18, 44.38, and 64.57 correspond to the Au PDF#99-056 card (Figure 2D). The XRD results further indicated that the dominant crystal structure within the catalyst was Au and NiO, as the depth of the XPS test was 5–10 nm, and the depth of the XRD test was 10–30 nm, which was also entirely consistent with the results of TEM lattice diffraction fringe. The XPS and XRD results suggested that the Au and NiO were successfully anchored to the carbon cloth surface. Electron paramagnetic resonance (EPR) was utilized to examine both Au-Vo-NiO/CC and Vo-NiO/CC catalysts to verify the presence of oxygen vacancies (g = 2.002) (Figure 2E).[7,37] The absorption intensity of Au-Vo-NiO/CC was slightly lower than that of Vo-NiO/CC, showing that some of the oxygen vacancies in Au-Vo-NiO/CC were occupied by Au atoms.[34,38] XPS is one of the most straightforward methods to detect oxygen vacancies. For this purpose, we analyzed the high-resolution spectra of the O 1*s* orbital

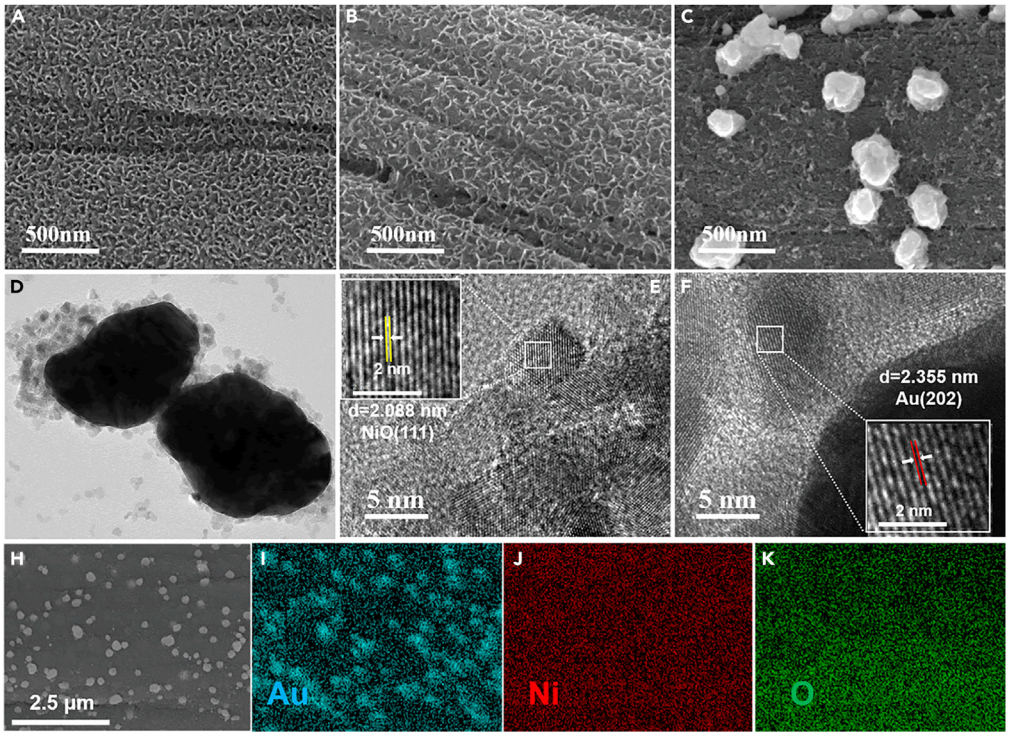

Figure 1. Structural and morphological characterization of Au-Vo-NiO/CC

(A–C) SEM images of $Ni(OH)_2$/CC, Vo-NiO/CC, and Au-Vo-NiO/CC.

(D–F) Illustration of the HRTEM image and corresponding FFT pattern of the Au-Vo-NiO/CC nanocatalyst.

(H–K) Elemental mapping images of Au-Vo-NiO/CC.

during the synthesis process in NiO/CC, Vo-NiO/CC, and Au-Vo-NiO/CC. In NiO/CC, the O 1*s* appears as a single peak, but after reduction with sodium borohydride, oxygen vacancies are created, and the O 1*s* is split into two peaks, which can be attributed to Ni-O and oxygen vacancies. After the *in situ* growth of Au, the O 1*s* experiences a 0.2 eV chemical shift, indicating that some of the O has been reduced (Figure S4). ICP experimental data were used to determine the contents of Ni (5.28%) and Au (0.77%) in the samples. An 8 h stability test was carried out on the catalyst sample, resulting in almost maintained Au content (0.67%) and depicting the stability characteristics of the Au-Vo-NiO/CC (Figure 2F).

Electrocatalytic performance

In a single-cell electrolytic system, a solution of 1M KOH and 0.5M formaldehyde was used as the reaction fluid, with Au-Vo-NiO/CC as the working electrode, a carbon rod as the counter electrode, and Hg/HgO as the reference electrode, forming a three-electrode system to test the FOR catalytic performance of Au-Vo-NiO/CC (Figure S5). Comparative analysis of Au-Vo-NiO/CC and NiO/CC demonstrated that the potential of the former was 0.47 V when the current density reached 50 mA cm^{-2}. In contrast, NiO/CC needed a higher driving potential at 1.45 V to achieve the same current density. The overpotential of NiO/CC is 0.22 V relative to the OER reaction, which means there is no catalytical activity for NiO to drive the FOR (Figures 3A and 3B). A parallel comparison with Au/CC showed that Au-Vo-NiO/CC triggered the FOR at a nearly identical potential as Au/CC, demonstrating Au as the core active catalytic site for the FOR. We compared the LSV curves of Au/CC and Au-Vo-NiO/CC and found that Au-Vo-NiO/CC had a faster growth rate than Au/CC. The potential difference between the two increased from 0.29 V to 0.56 V when the current density increased from 50 to 100 mA cm^{-2}. The superior electrocatalytic performance of Au-Vo-NiO/CC was attributed to the catalytic activity of Au for the FOR reaction, as well as the enhanced electron transfer rate and active site number by NiO and oxygen vacancies. We further investigated the mass transfer changes during the reaction process by measuring the EIS spectra at different potentials. The results showed negligible electron transfer between the electrodes when the potential was between −0.1 and 0.1 V (vs. RHE), as indicated by the high resistance (Rct) values ranging from 350 to 100 Ω. The Rct value dropped sharply to 35 Ω when the potential rose to 0.2 V (vs. RHE), signifying the onset of the reaction. The Rct value decreased further to around 10 Ω when the potential rose above 0.3 V (vs. RHE), suggesting a high electron transfer rate on the catalyst surface (Figure S6; and Tables S1–S9).

The comparative testing for LSV curves was then carried out on Au-Vo-NiO/CC in different systems, with or without the addition of formaldehyde. The FOR occurred on the anodic side at low potentials when formaldehyde was present. In the absence of formaldehyde, the anodic side mainly carried out the OER in the system (Figures 3C and 3D). The FOR has a competitive advantage over OER owing to its lower driving potential, and the reaction system is accordingly more inclined to the FOR pathway. The energy-saving effect of the Au-Vo-NiO/CC

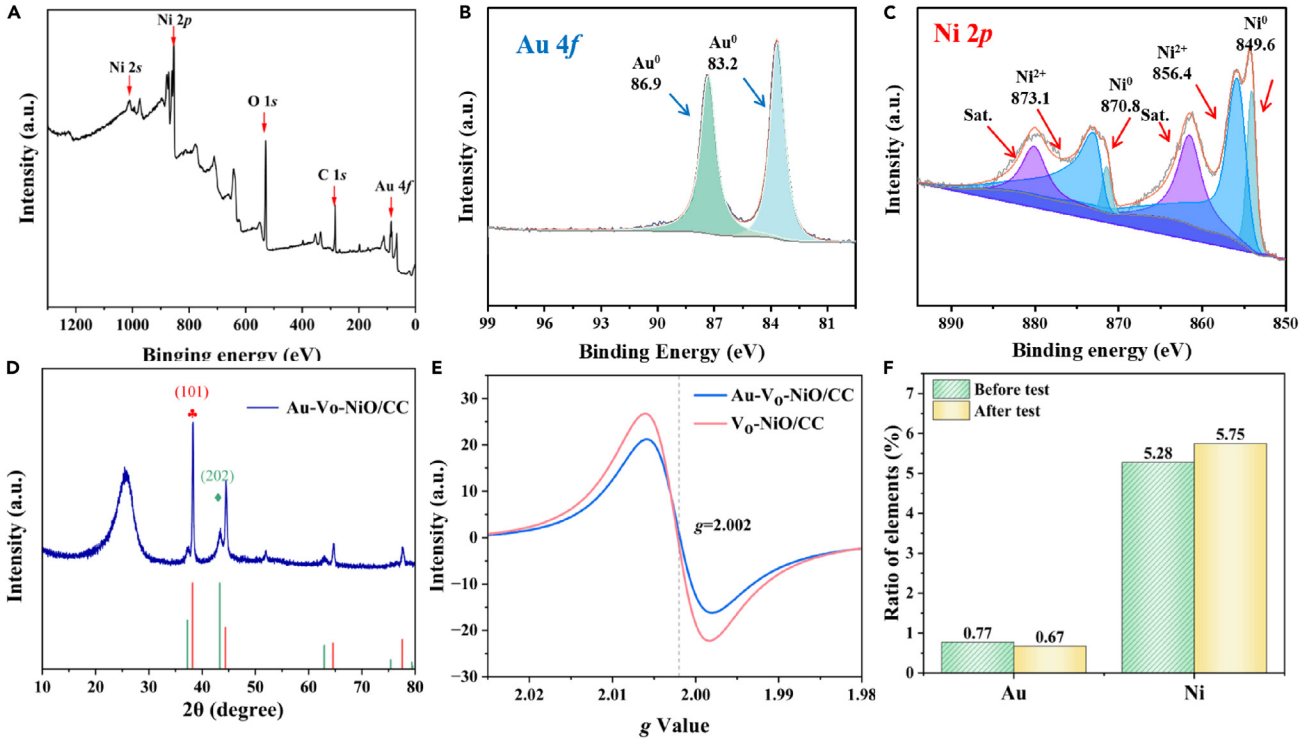

Figure 2. Characterization of the material composition of Au-Vo-NiO/CC

(A) XPS spectra of Au-Vo-NiO/CC.

(B and C) High-resolution Au 4*f* and Ni 2*p* XPS spectra.

(D) XRD pattern of Au-Vo-NiO/CC.

(E) EPR patterns of different electrocatalysts.

(F) Au and Ni contents before and after long-term stability testing.

catalyst was investigated at current densities of 0, 50, 100, 150, 200, 250, and 300 mA cm^{-2} (Figure 3E). The results showed that energy-saving efficiency was nearly 80% at low current density, and this trend attenuated with increasing current density. With the current density reaching 300 mA cm^{-2}, the OER pathway gradually dominated, maintaining an energy-saving efficiency of over 40%. The catalytic performance of Au-Vo-NiO/CC for HER was also evaluated (Figure 3F), and it could drive the reaction at −0.18 V. At this point, Au-Vo-NiO/CC demonstrated a perfect dual FOR and HER catalytic performance.

We performed the following experiments to analyze the products of the FOR and HER reactions and investigate the bifunctional catalytic characteristics of Au-Vo-NiO/CC. We used an H-type divided electrolytic cell with 1 M KOH and 0.5 M formaldehyde as the electrolyte and Au-Vo-NiO/CC as the working and counter electrodes. The reference electrode was Hg/HgO (Figure S7). We used ion chromatography (IC) to detect the liquid phase products and GC-MS and DEMS to detect the gaseous products. We used volumetric displacement to quantify the gaseous products and ^{1}H-NMR to qualitatively identify the liquid-phase organic products (Figure S8). The potential difference between HER&FOR and conventional HER&OER was contrasted. The potential on the anode side of HER&FOR has a severe drop at a current density of 50 mA cm^{-2} (ΔE = 1.13 V). This potential advantage does not weaken significantly as the current density increases (ΔE = 1.10 V @ 100 mA cm^{-2}) (Figure 4A). Subsequently, the gas phase products on the anode side were analyzed by DEMS detection. To avoid the competition between FOR and ORE at excessively high potentials, an intermittent DE-MS test was performed at a potential of 0.3V (the current density is approximately 15 mA cm^{-2}) (Figure S9). A solution of 1 M NaOD (D_2O) + HCHO were applied instead to clarify the source of the H-atom for H_2 production. Several channels [m/z = 2 (H_2), 3 (HD), 4 (D_2) and 44 (CO_2)] were collected and analyzed separately for the gas phase products of FOR. No CO_2, HD or D_2 generation was observed, and the main product was verified as H_2 for 50 s at an applied potential of 0.3 V. It indicated that H_2 was produced via the catalytic oxidation of HCHO. (Figure 4B) The liquid phase products of FOR were analyzed by IC, and formaldehyde was mainly converted to formate (Figure 4C). To verify the catalytic efficiency of Au-Vo-NiO/CC as a FOR electrocatalyst, the formate concentration and hydrogen yield on the anode side with constant current (i-t) in long-time (V = 0.5 V vs. RHE) were examined. The FE was calculated accordingly and indicated nearly 100% efficiency for formate and H_2 (Figure 4D). It demonstrated that the Au-Vo-NiO/CC electrode has a high selectivity for formaldehyde oxidation. Constant electric potential experiments were carried out at different values, highlighting the effect of the electric potential. The reaction statistics were immediately collected at a flux of 100 C. By monitoring the formate concentration, the FE of formic acid was calculated to be ~100% when the electric potential was 1.0–1.5 V (Figure 4E). As the potential continued to increase, the FE of formic acid showed a downward trend, indicating a competition between FOR and OER at a high electric

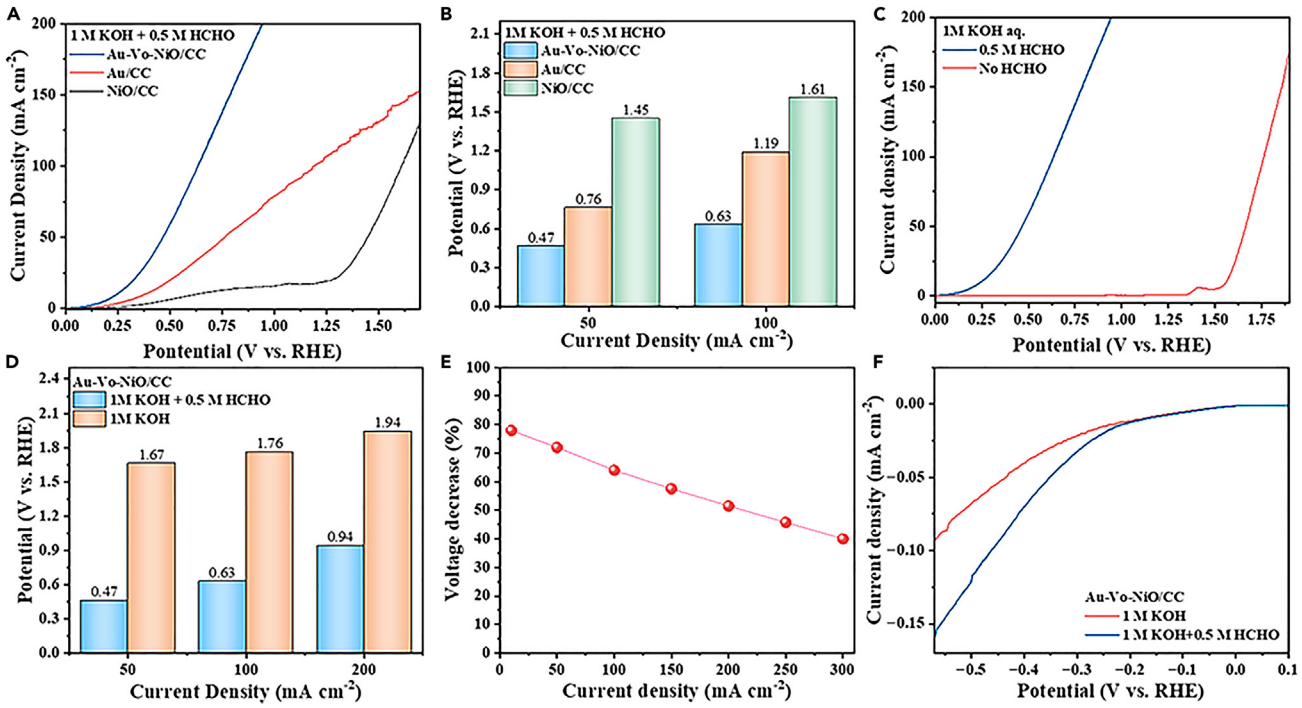

Figure 3. The study of the electrocatalytic performance of Au-Vo-NiO/CC under a three-electrode single-cell electrolysis system

(A) Linear sweep voltammetry (LSV) curves of Au-Vo-NiO/CC, Au/CC, and NiO/CC anodes in 1.0 M KOH containing 0.5 M formaldehyde.

(B) Potentials at 50 and 100 mA cm^{-2}.

(C) LSV curves of Au-Vo-NiO/CC anode in 1.0 M KOH with or without 0.5 M formaldehyde.

(D) Potentials at 50 and 100 mA cm^{-2}.

(E) The energy consumption savings of FOR at different current densities.

(F) LSV curves of Au-Vo-NiO/CC cathode for HER in 1.0 M KOH with or without 0.5 M formaldehyde.

potential. The stability of the catalyst is an essential factor that could dramatically impact the catalytic efficiency. A long-term experiment of Au-Vo-NiO/CC in FOR&HER was then conducted, showing that the current density decreased gradually with the drop in formaldehyde concentration. However, the system could be refreshed to the initial state when the formaldehyde concentration is recovered during the 8 h experiment (Figure 4F). LSV analysis for the catalyst before or after the long-time stability experiment showed a high-degree overlap between the curves (Figure 4G). In addition, an analysis of the conversion rate of the products after a long-term complete reaction was conducted. The results showed that the current decayed to near zero after a 45-h long i-t test. Upon detection of the formate content in the solution using IC, it was found that the conversion rate from reactant to product was 94.2% (Figure S10). It could be concluded that Au-Vo-NiO/CC has excellent stability behavior as a FOR&HER catalyst.

The *in situ* Raman spectroscopy was used to track and monitor the reaction at different electric potentials (Figure 4G). When the potential reached 0.45 V (vs. RHE), the bands at 520, 900, and 1031 cm^{-1} emerged, corresponding separately to the C-O bending vibrational, symmetric, and anti-symmetric modes.[39] The absorption intensity is augmented as the electric potential value increases. This suggested that Au-Vo-NiO/CC could initiate the formation of *HCOOH intermediate from formaldehyde at low electric potentials. The absorption at 1250 cm^{-1} and 1480 cm^{-1}, corresponding to the O-H bending mode, became more evident with increasing potential value.[40] This result indicated that the O-H bond in *HCOOH was generally broken, confirming that formaldehyde is an H-donor throughout the catalytic H_2 production reaction.

DFT calculations

For further understanding of the mechanistic rationale, density functional theory (DFT) was used to calculate the energy profiles for HCHO oxidation and H_2 production (Figures 5D and S11–S13). The result showed that Au nanoparticles anchored on NiO had the minimum activation energy barrier (0.49 eV and 0.18 eV, respectively), indicating that Au species served as the leading active site in the prepared catalysts. The simulations on the pathway revealed that the formation of *CHO intermediate was the rate-determining step. The calculated charge density difference mappings showed that more transferred charges were aggregated in the interface between *CHO and NiO-supported Au nanoparticles, efficiently stabilizing the intermediate (Figures 5A and 5B). Moreover, the projected density of state (PDOS) showed that the interaction between Au nanoparticle and NiO inclined the Au 5*d*ays states to a more negative region than those anchored directly on the carbon surface (Figure 5C). This negative shift promised the NiO-supported Au nanoparticles an enhanced bonding affinity for stabilizing

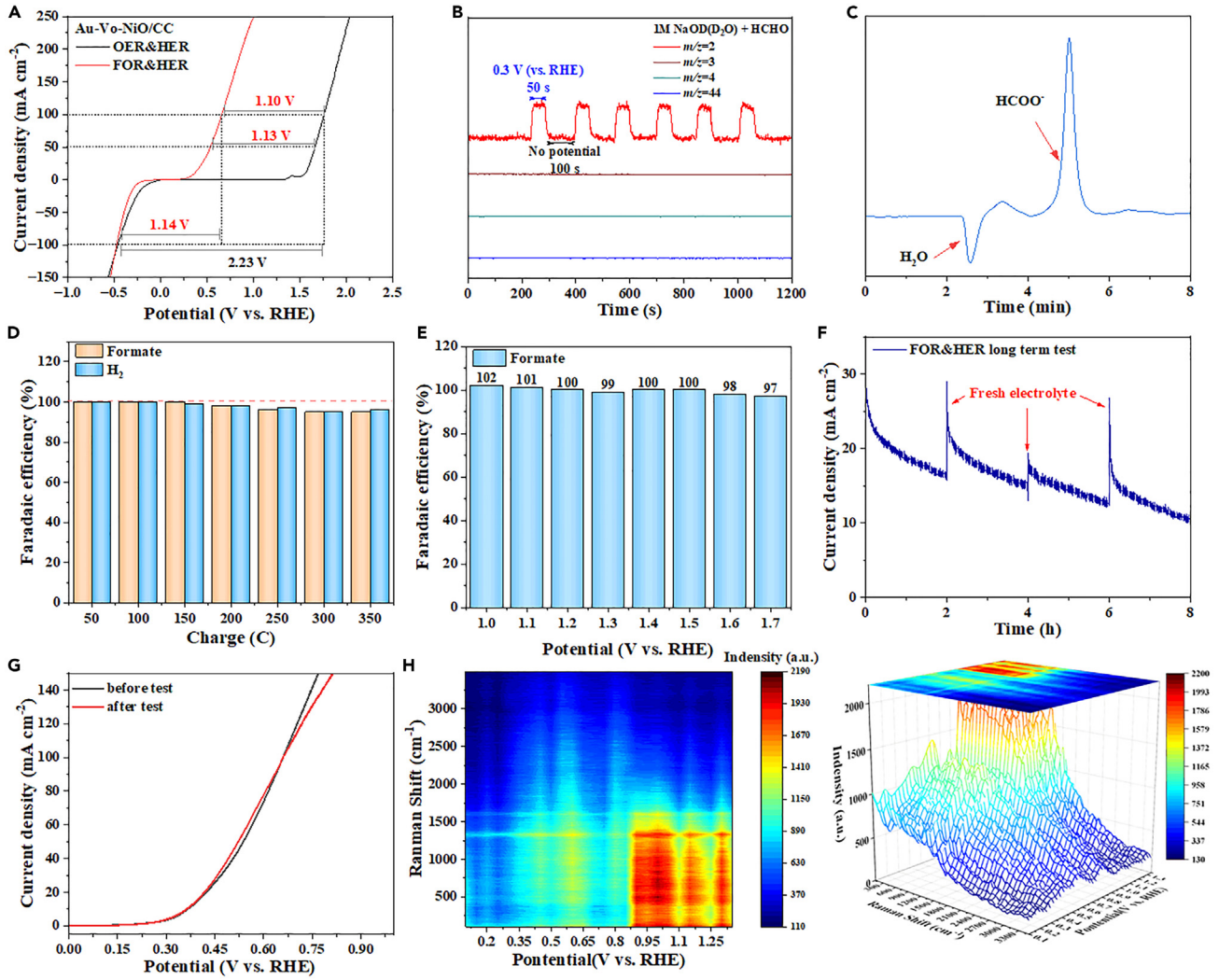

Figure 4. Au-Vo-NiO/CC simultaneously catalyzes FOR and HER in an H-type electrolytic cell

(A) The LSV curve in a 1.0M KOH solution with or without a 0.5M formaldehyde.

(B) DEMS signals at m/z = 2, 3, 4, and 44 at the pulsed potential of 0.3 V (vs. RHE) over the Au-Vo-NiO/CC in 1.0 M NaOD with 0.5 M HCHO using D_2O as the electrolyte solvent.

(C) The chromatographic curves of formate measured by IC on the anode under a cell potential of 0.50 V (vs. RHE) for Au-Vo-NiO/CC.

(D and E) The calculated Faraday efficiencies of formate and H_2.

(F) The Long-term stability of Au-Vo-NiO/CC.

(G) The LSV curves before and after the i-t test.

(H) The *In situ* Raman spectroscopy of the Au-Vo-NiO/CC electrode for 1.0 M KOH with 0.5 M formaldehyde.

*CHO via Au-C bonding. It also indicated that the support-metal interaction via NiO could effectively tune the electronic and catalytic properties of the anchored Au nanoparticles. In addition, an interaction between the newly formed HCOOH and the electrode surface was observed, which might intercept further oxidation into CO_2.

Conclusion

In summary, the electrocatalyst Au-Vo-NiO/CC was synthesized for the oxidative H_2 production of formaldehyde at ultra-low potentials. The design mainly focused on increasing the interaction tendency between O-atom and IB elements from Cu to Au. Experimental results highlight that the bipolar H_2 production mode can be driven at 0.2 V (vs. RHE), and the Faraday efficiency of H_2 production at both the cathode and anode is close to 100%. On the cathode side, formaldehyde is partially oxidized to afford formate as an added-value byproduct. The presented system dramatically reduces the energy consumption of water electrolysis (by about 40%–80%), efficiently boosting the economic value of the FOR&HER protocol. DFT calculations reveal that generating *CHO intermediate is the rate-determining step, and

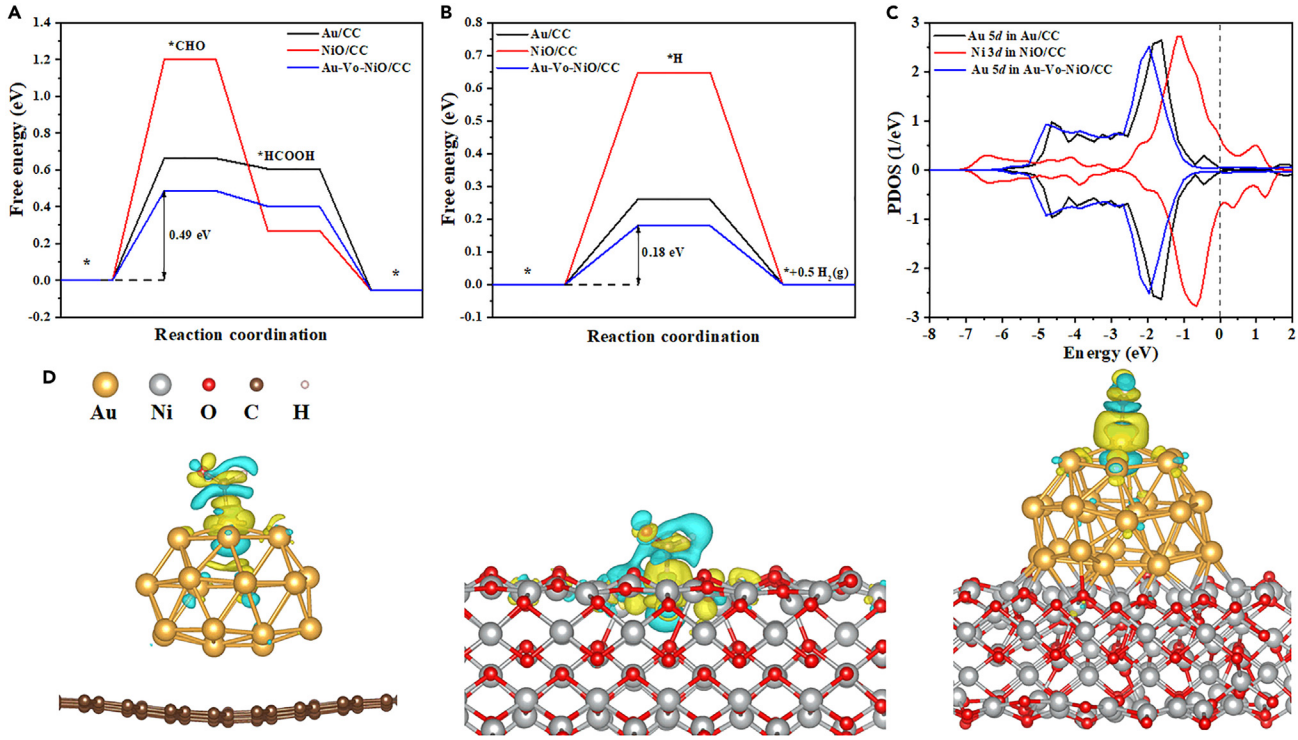

Figure 5. Calculated energy profiles

(A) HCHO oxidation.

(B) Hydrogen production.

(C) PDOS of reaction sites in Au/CC, NiO, and Au-Vo-NiO. The dashed lines stand for the Fermi level.

(D) Illustrations of the mechanism for the formaldehyde oxidation process in different catalysts.

the Au-Vo-NiO/CC has the minimum energy barrier compared to the monometallic catalysts (Au or Ni). Follow-up work in our laboratory will focus on the application scenarios of this newly designed electrocatalyst, also involving studies on some other metal-doped electrodes for the bipolar H_2 production protocols.

Limitations of the study

This study has shown that Au is the leading active site for the electrocatalytic oxidation of formaldehyde, but the role of Ni and oxygen vacancies on the catalytic activity of Au remains unclear. Future work can address this gap by characterizing the material structure and properties of Au-Vo-NiO/CC and providing more evidence to support the proposed catalytic mechanism. This would make the research more comprehensive and convincing.

STAR★METHODS

Detailed methods are provided in the online version of this paper and include the following:

- KEY RESOURCES TABLE
- RESOURCE AVAILABILITY
  - Lead contact
  - Materials availability
  - Date and code availability
- EXPERIMENTAL MODEL AND SUBJECT DETAILS
- METHOD DETAILS
  - Materials
  - Treatment of the carbon cloth (CC)
  - Synthesis of the precursor $Ni(OH)_2$/CC
  - Synthesis of the precursor NiO/CC
  - Synthesis of the Vo-NiO/CC

- Synthesis of the Au-Vo-NiO/CC
- Synthesis of the Au/CC catalyst
- Material characterization
- Electrochemical measurements
- Product analysis
- Density functional theory (DFT) calculations

- QUANTIFICATION AND STATISTICAL ANALYSIS
- ADDITIONAL RESOURCES

SUPPLEMENTAL INFORMATION

Supplemental information can be found online at https://doi.org/10.1016/j.isci.2023.107994.

ACKNOWLEDGMENTS

This work was funded by the Guangdong Basic and Applied Basic Research Foundation (2021A1515110352, 2022A1515010916, 2023A1515011629), Shandong Provincial Natural Science Foundation (ZR2021QB067), and Shenzhen Science and Technology Innovation Commission (KCXFZ20201221173404013). We are grateful to the Shenzhen Bay Laboratory Supercomputing Center for the assistance in DFT calculation.

AUTHOR CONTRIBUTIONS

Methodology, Y.Z., Z.L., Q.Y., J.W., Z.R., J.Z., and J.C.; Investigation, Y.Z., Z.L., Q.Y., J.W., Z.R., J.Z., and J.C.; Writing - Original Draft, Y.Z. and Z.L.; Writing - Review & Editing, J.Z. and J.C.; Supervision, J.Z. and J.C.

DECLARATION OF INTERESTS

The authors declare no conflict of interest.

INCLUSION AND DIVERSITY

We support inclusive, diverse, and equitable conduct of research.

Received: June 21, 2023
Revised: July 6, 2023
Accepted: September 18, 2023
Published: September 22, 2023

REFERENCES

1. Wang, Y., Zhou, W., Wang, J., Karaesmen, E., Tang, H., McCarthy, P.L., Pasquini, M.C., Wang, Y., McReynolds, L.J., Katki, H.A., et al. (2021). Combined anodic and cathodic hydrogen production from aldehyde oxidation and hydrogen evolution reaction. Blood Adv. *5*, 66–70.
2. Lee, J.E., Jeon, K.J., Show, P.L., Lee, I.H., Jung, S.C., Choi, Y.J., Rhee, G.H., Lin, K.Y.A., and Park, Y.K. (2022). Mini review on H_2 production from electrochemical water splitting according to special nanostructured morphology of electrocatalysts. Fuel *308*, 122048.
3. Xiong, B., Zhao, W., Tian, H., Huang, W., Chen, L., and Shi, J. (2022). Nickel-tungsten nano-alloying for high-performance hydrogen electrocatalytic oxidation. Chem. Eng. J. *432*, 134189.
4. Kang, X., Yang, F., Zhang, Z., Liu, H., Ge, S., Hu, S., Li, S., Luo, Y., Yu, Q., Liu, Z., et al. (2023). A corrosion-resistant RuMoNi catalyst for efficient and long-lasting seawater oxidation and anion exchange membrane electrolyzer. Nat. Commun. *14*, 3607.
5. Wang, Y., Wang, M., Yang, Y., Kong, D., Meng, C., Zhang, D., Hu, H., and Wu, M. (2023). Potential technology for seawater electrolysis: Anion-exchange membrane water electrolysis. Chem Catal. *3*, 100643–100674.
6. Yu, Z.Y., Duan, Y., Feng, X.Y., Yu, X., Gao, M.R., and Yu, S.H. (2021). Clean and affordable hydrogen fuel from alkaline water splitting: past, recent progress, and future prospects. Adv. Mater. *33*, e2007100.
7. Wu, X., Zhang, Y., Yang, Y., Fu, G., Si, F., Chen, J., Ahmad, M., Zhang, Z., Ye, C., Zhang, J., et al. (2023). Ni_2P with phosphorus vacancy supported Pt clusters for efficiently electrocatalytic co-production of hydrogen and value-added chemicals from methanol-water at low potential. Chem. Eng. J. *452*, 139057.
8. Zhang, F., and Wang, Q. (2021). Redox-mediated water splitting for decoupled H_2 production. ACS Mater. Lett. *3*, 641–651.
9. Zhao, Y., Adiyeri Saseendran, D.P., Huang, C., Triana, C.A., Marks, W.R., Chen, H., Zhao, H., and Patzke, G.R. (2023). Oxygen Evolution/reduction reaction catalysts: from *in situ* monitoring and reaction mechanisms to rational design. Chem. Rev. *123*, 6257–6358. https://doi.org/10.1021/acs.chemrev.6257-6358.
10. Li, S., Li, Z., Ma, R., Gao, C., Liu, L., Hu, L., Zhu, J., Sun, T., Tang, Y., Liu, D., and Wang, J. (2021). A glass-ceramic with accelerated surface reconstruction toward the efficient oxygen evolution reaction. Angew. Chem. Int. Ed. *60*, 3773–3780.
11. Guo, X., Wan, X., Liu, Q., Li, Y., Li, W., and Shui, J. (2022). Phosphated Ir-Mo bimetallic cluster for efficient hydrogen evolution reaction. eScience *2*, 304–310.
12. Zhao, B., Liu, J., Wang, X., Xu, C., Sui, P., Feng, R., Wang, L., Zhang, J., Luo, J.L., and Fu, X.Z. (2021). CO_2-emission-free electrocatalytic CH_3OH selective upgrading with high productivity at large current densities for energy saved hydrogen co-generation. Nano Energy *80*, 105530.
13. Li, S., Ma, R., Hu, J., Li, Z., Liu, L., Wang, X., Lu, Y., Sterbinsky, G.E., Liu, S., Zheng, L., et al. (2022). Coordination environment tuning of nickel sites by oxyanions to optimize methanol electro-oxidation activity. Nat. Commun. *13*, 2916–2927.
14. Chen, J., Ahmad, M., Zhang, Y., Ye, H., Wang, L., Zhang, J., Fu, X.Z., and Luo, J.L. (2023). Versatile Mo modulation effects enable efficient electrocatalytic aqueous methanol

electro-reforming over surface-engineered NiCoMo alloy. Chem. Eng. J. *454*, 140056.
15. Kumar, A., Daw, P., and Milstein, D. (2022). Homogeneous catalysis for sustainable energy: hydrogen and methanol economies, fuels from biomass, and related topics. Chem. Rev. *122*, 385–441.
16. Zhang, J., Qu, X., Han, Y., Shen, L., Yin, S., Li, G., Jiang, Y., and Sun, S. (2020). Engineering PtRu bimetallic nanoparticles with adjustable alloying degree for methanol electrooxidation: Enhanced catalytic performance. Appl. Catal., B *263*, 118345.
17. Kang, K.N., Kim, S.I., Yoon, J.C., Kim, J., Cahoon, C., and Jang, J.H. (2022). Bi-functional 3D-NiCu-double hydroxide@partially etched 3D-NiCu catalysts for non-enzymatic glucose detection and the hydrogen evolution reaction. ACS Appl. Mater. Interfaces *14*, 33013–33023.
18. Li, Y., Wei, X., Chen, L., Shi, J., and He, M. (2019). Nickel-molybdenum nitride nanoplate electrocatalysts for concurrent electrolytic hydrogen and formate productions. Nat. Commun. *10*, 5335–5347.
19. Deng, X., Xu, G.Y., Zhang, Y.J., Wang, L., Zhang, J., Li, J.F., Fu, X.Z., and Luo, J.L. (2021). Understanding the roles of electrogenerated Co^{3+} and Co^{4+} in selectivity-tuned 5-hydroxymethylfurfural oxidation. Angew. Chem. Int. Ed. *60*, 20535–20542.
20. Chen, L., Wang, Y., Li, S., Zhou, W., and Sun, L. (2021). Co-electrolysis toward value-added chemicals. Arthroplasty *3*, 1–9.
21. Gao, G., Remón, J., Jiang, Z., Yao, L., and Hu, C. (2022). Selective hydrogenation of furfural to furfuryl alcohol in water under mild conditions over a hydrotalcite-derived Pt-based catalyst. Appl. Catal. B *309*, 122160.
22. Wang, L., Zhu, Y., Wen, Y., Li, S., Cui, C., Ni, F., Liu, Y., Lin, H., Li, Y., Peng, H., and Zhang, B. (2021). Regulating the local charge distribution of Ni active sites for the urea oxidation reaction. Angew. Chem. Int. Ed. *60*, 10577–10582.
23. Zhang, Y., Qiu, Y., Wang, Y., Li, B., Zhang, Y., Ma, Z., and Liu, S. (2021). Coaxial Ni-S@N-doped carbon nanofibers derived hierarchical electrodes for efficient H_2 production via urea electrolysis. ACS Appl. Mater. Interfaces *13*, 3937–3948.
24. Si, F., Liu, J., Zhang, Y., Zhao, B., Liang, Y., Wu, X., Kang, X., Yang, X., Zhang, J., Fu, X., and Luo, J. (2023). Surface spin enhanced high stable $NiCo_2S_4$ for energy-saving production of H_2 from water/methanol coelectrolysis at high current density. Small *19*, e2205257.
25. Li, G., Han, G., Wang, L., Cui, X., Moehring, N.K., Kidambi, P.R., Jiang, D.E., and Sun, Y. (2023). Dual hydrogen production from electrocatalytic water reduction coupled with formaldehyde oxidation via a copper-silver electrocatalyst. Nat. Commun. *14*, 525–536.
26. Pan, Y., Li, Y., Dong, C.L., Huang, Y.C., Wu, J., Shi, J., Lu, Y., Yang, M., Wang, S., and Zou, Y. (2023). Unveiling the synergistic effect of multi-valence Cu species to promote formaldehyde oxidation for anodic hydrogen production. Chem *9*, 963–977.
27. Yang, Y., Wu, X., Ahmad, M., Si, F., Chen, S., Liu, C., Zhang, Y., Wang, L., Zhang, J., Luo, J.L., and Fu, X.Z. (2023). A direct formaldehyde fuel cell for CO_2-emission free Co-generation of electrical energy and valuable chemical/hydrogen. Angew. Chem. Int. Ed. *62*, e202302950.
28. Wang, C., Li, Y., Zhang, C., Chen, X., Liu, C., Weng, W., Shan, W., and He, H. (2021). A simple strategy to improve Pd dispersion and enhance Pd/TiO_2 catalytic activity for formaldehyde oxidation: The roles of surface defects. Appl. Catal., B *282*, 119540.
29. Han, G., Li, G., and Sun, Y. (2023). Electrocatalytic dual hydrogenation of organic substrates with a Faradaic efficiency approaching 200%. Nat. Catal. *6*, 224–233.
30. Sherbo, R.S., and Kurimoto, A. (2023). Doubling the efficiency of electrosynthesis. Nat. Catal. *6*, 218–219.
31. Yuan, Q., Yang, Y., Gong, S., Chen, S., Huang, M., Wang, C., Tong, H., and Chen, Q. (2021). RuNi alloy nanoparticles encapsulated in oxygen-doped carbon as bifunctional catalyst towards hydrogen electrocatalysis. Chin. J. Chem. *39*, 3455–3461.
32. Zhang, P., and Sun, L. (2020). Electrocatalytic hydrogenation and oxidation in aqueous conditions. Chin. J. Chem. *38*, 996–1004.
33. Tang, Y.J., and Lan, Y.Q. (2023). Rational design and synthesis of advanced metal-organic frameworks for electrocatalytic water splitting. Sci. China Chem. *66*, 943–965.
34. Xiao, Z., Huang, Y.C., Dong, C.L., Xie, C., Liu, Z., Du, S., Chen, W., Yan, D., Tao, L., Shu, Z., et al. (2020). Operando identification of the dynamic behavior of oxygen vacancy-rich Co_3O_4 for oxygen evolution reaction. J. Am. Chem. Soc. *142*, 12087–12095.
35. Hui, L., Zhang, X., Xue, Y., Chen, X., Fang, Y., Xing, C., Liu, Y., Zheng, X., Du, Y., Zhang, C., et al. (2022). Highly dispersed platinum chlorine atoms anchored on gold quantum dots for a highly efficient electrocatalyst. J. Am. Chem. Soc. *144*, 1921–1928.
36. Pal, D., Sarkar, A., Ghosh, N.G., Sanke, D.M., Maity, D., Karmakar, K., Sarkar, D., Zade, S.S., and Khan, G.G. (2021). Integration of $LaCo(OH)_x$ photo-electrocatalyst and plasmonic gold nanoparticles with Sb-doped TiO_2 nanorods for photoelectrochemical water oxidation. ACS Appl. Nano Mater. *4*, 6111–6123.
37. Xiao, Z., Wang, Y., Huang, Y.C., Wei, Z., Dong, C.L., Ma, J., Shen, S., Li, Y., and Wang, S. (2017). Filling the oxygen vacancies in Co_3O_4 with phosphorus: an ultra-efficient electrocatalyst for overall water splitting. Energy Environ. Sci. *10*, 2563–2569.
38. Xiang, K., Song, Z., Wu, D., Deng, X., Wang, X., You, W., Peng, Z., Wang, L., Luo, J.L., and Fu, X.Z. (2021). Bifunctional $Pt–Co_3O_4$ electrocatalysts for simultaneous generation of hydrogen and formate via energy-saving alkaline seawater/methanol co-electrolysis. J. Mater. Chem. A *9*, 6316–6324.
39. Qian, K., Du, L., Zhu, X., Liang, S., Chen, S., Kobayashi, H., Yan, X., Xu, M., Dai, Y., and Li, R. (2019). Directional oxygen activation by oxygen-vacancy-rich WO_2 nanorods for superb hydrogen evolution via formaldehyde reforming. J. Mater. Chem. A *7*, 14592–14601.
40. Du, L., Qian, K., Zhu, X., Yan, X., Kobayashi, H., Liu, Z., Lou, Y., and Li, R. (2019). Interface engineering of palladium and zinc oxide nanorods with strong metal–support interactions for enhanced hydrogen production from base-free formaldehyde solution. J. Mater. Chem. A *7*, 8855–8864.

STAR★METHODS

KEY RESOURCES TABLE

REAGENT or RESOURCE	SOURCE	IDENTIFIER
Chemicals, peptides, and recombinant proteins		
$Ni(NO_3)_2{\cdot}6H_2O$	Aladdin Co., Ltd	CAS: 13478-00-7
$KAuCl_4$	Aladdin Co., Ltd	CAS: 13682-61-6
Formaldehyde	Xilong Scientific	CAS: 50-00-0

RESOURCE AVAILABILITY

Lead contact

Further information and requests for resources should be directed to and will be fulfilled by the lead contact, Jiean Chen (chenja@szbl.ac.cn).

Materials availability

This study did not generate new unique reagents.

Date and code availability

The lead contact will share all data reported in this paper upon request.
This paper does not report original code.
Any additional information required to reanalyze the data reported in this paper is available from the lead contact upon request.

EXPERIMENTAL MODEL AND SUBJECT DETAILS

This study does not use experimental models.

METHOD DETAILS

Materials

$Ni(NO_3)_2{\cdot}6H_2O$ (nickelous nitrate, 99.99%, AR grade) and $KAuCl_4$ (Potassium gold(III) chloride, 98%, AR grade) all are purchased from Aladdin Ltd (Shanghai, China). The carbon cloth (CC) used in this research is from Carbon Energy in Taiwan (Taiwan, China). Formaldehyde (GR, 38%) was purchased from Xilong Scientific.

Treatment of the carbon cloth (CC)

The CC was immersed in aqueous 1.0 M nitric acid for 1 h. Then it was taken out and cleaned thoroughly with deionized water (DIW). After calcination at 350°C for 3 h in a muffle furnace, it was cooled to room temperature and stored in a dry oven at 60°C.

Synthesis of the precursor $Ni(OH)_2$/CC

Pretreated carbon cloth was used as the working electrode, a platinum sheet was used as the counter electrode, and a Saturated Calomel Electrode (SCE) was used as the reference electrode. The carbon cloth grown with $Ni(OH)_2$ nano-sheets was electrodeposited in 0.1 M $Ni(NO_3)_2$ aqueous solution at a potential of -1.0 V (vs. SCE) for 500 sec. Then the prepared carbon cloth was washed repeatedly with DIW and ethanol and stored in a dry oven at 60°C.

Synthesis of the precursor NiO/CC

The prepared $Ni(OH)_2$/CC was placed in a muffle furnace and calcined at 350°C for 3 h. When $Ni(OH)_2$ was oxidized completely to NiO, the calcination was stopped and cooled to room temperature to complete the preparation of NiO/CC.

Synthesis of the Vo-NiO/CC

To obtain NiO nano-sheet catalysts with oxygen vacancies, the prepared NiO/CC was immersed in 0.1 M $NaBH_4$ aqueous solution for 5 min and then the solution was discarded and the Vo-NiO/CC was washed with DIW. Then the product was stored in a dry oven.

Synthesis of the Au-Vo-NiO/CC

The prepared Vo-NiO/CC was immersed in an aqueous $KAuCl_4$ (0.1 mM) solution for 2 h. After removal, it was rinsed with DIW and dried in an oven to obtain the final Au-Vo-NiO/CC electrocatalyst product.

Synthesis of the Au/CC catalyst

The Au/CC catalyst was prepared by the hydrothermal method and used as a control species. The CC was placed in a hydrothermal kettle, 30 mL aqueous $AuCl_4K$ (40 mM) was added, and the hydrothermal reaction proceeded at 120°C for 12 h. When the reaction was completed, the Au/CC catalyst was rinsed well and stored in an oven at 60°C.

Material characterization

The morphology and microstructure were characterized using field emission scanning electron microscopy (TESCAN MIRA LMS, Czech Republic) and field emission transmission electron microscopy (FEI Tecnai F20, USA). The X-ray diffraction (XRD) pattern was obtained using a Rigaku Miniflex 600 instrument (Japan). Detailed analysis of the elemental composition was conducted using X-ray photoelectron spectroscopy (XPS), performed on a Thermo Scientific Nexsa instrument (USA) with an Al Kα radiation excitation source (hν = 1486.6 eV). ICP-OES/MS.

Electrochemical measurements

All electrochemical measurements are conducted at room temperature using an electrochemical workstation (CHI650E, Chenhua Instrument Company, Shanghai). Electrochemical measurements are carried out in a three-electrode system. Foam Nickel (1×1 cm^2) is used as the working electrode; mercury oxide is the reference electrode, and platinum mesh (1×1 cm^2) is the counter electrode. All potentials are calibrated as reversible hydrogen electrodes (RHE):

$$E_{RHE} = E_{Hg/HgO} + 0.059\ pH + 0.098$$

Impedance spectrum measurement is conducted from 1000000 Hz to 0.01 Hz at an open circuit potential.

Product analysis

Ion chromatography (Technology Co. Ltd., Qingdao, China), which was equipped with organic anion columns containing the leachate of 2.4 mmol Na_2CO_3 and 6 mmol $NaHCO_3$, was employed for the quantification of products from electrochemical oxidation of methanol. Before chronoamperometry measurements, 100 μL of electrolyte was collected and diluted with DIW with a ratio of 1:100. The measurement of each sample was repeated three times, and the concentration of formate ion was calibrated based on standard solutions with known concentrations. The detailed calculations for the Faradaic efficiency (FE) and energy consumption are listed in the supporting information.

The Faradaic efficiency (FE) of product formation was calculated based on the following equation:

$$FE\ \% = \frac{mole\ product\ produced \times n \times F}{Total\ chatge\ passed}$$

Where n is the number of electrons transferred for each production formation, and F is the Faraday constant (96,485 C/mol).

The calculation method for energy-saving efficiency of FOR compared to OER.

$$\text{Energy Consumption Savings} = \frac{E_{OER} - E_{FOR}}{E_{OER}}\ \%$$

Density functional theory (DFT) calculations

The energy profiles of converting HCHO into HCOOH and hydrogen were investigated on as-prepared catalysts by the Vienna Ab-initio Simulation Package (VASP) with the revised Perdew-Burke-Ernzerhof (RPBE) of the generalized gradient approximation (GGA). The interaction between ionic and valence electrons was described by PAW pseudo-potential. Considering the structural features of as-prepared catalysts, Au nanoparticle was built on carbon and NiO surfaces. A 4×6 carbon supercell simulated the carbon component, while the NiO surface was simulated by its typical (202) facet consisting of a 2×3 supercell containing six O-Ni-O layers. Au nanoparticle was simulated by a cluster model consisting of 31 Au atoms on the carbon layer or NiO surface. All geometry optimization calculations adopted the 1×10^{-4} eV energy convergence and cutoff energy of 400 eV at G point. The spin polarization was considered in the calculations of geometry optimization. After geometry optimization, the charge density difference mappings and projected density of state (PDOS) were calculated with the cutoff energy of 400 eV and energy convergence of 1×10^{-5} eV. The reported standard hydrogen electrode (SHE) model was used to calculate Gibbs free energy changes (ΔG) of all reaction steps at U = 0 V vs. SHE at pH = 0, which was used to evaluate the reaction barrier. The following formula calculated the G:

$$G=E + H(T) - TS$$

where E, H (T) and S are the electronic free energy, enthalpy and entropy of the model at T = 298.15 K, respectively.

QUANTIFICATION AND STATISTICAL ANALYSIS

This study does not include statistical analysis or quantification.

ADDITIONAL RESOURCES

This work does not include any additional resources.